

Convergence of a symmetric MPFA method on quadrilateral grids

I. Aavatsmark · G. T. Eigestad · R. A. Klausen ·
M. F. Wheeler · I. Yotov

Received: 21 October 2005 / Accepted: 19 March 2007 / Published online: 21 August 2007
© Springer Science + Business Media B.V. 2007

Abstract This paper investigates different variants of the multipoint flux approximation (MPFA) O-method in 2D, which rely on a transformation to an orthogonal reference space. This approach yields a system of equations with a symmetric matrix of coefficients. Different methods appear, depending on where the transformed permeability is evaluated. Midpoint and corner-point

evaluations are considered. Relations to mixed finite element (MFE) methods with different velocity finite element spaces are further discussed. Convergence of the MPFA methods is investigated numerically. For corner-point evaluation of the reference permeability, the same convergence behavior as the O-method in the physical space is achieved when the grids are refined uniformly or when grid perturbations of order h^2 are allowed. For h^2 -perturbed grids, the convergence of the normal velocities is slower for the midpoint evaluation than for the corner-point evaluation. However, for rough grids, i.e., grids with perturbations of order h , contrary to the physical space method, convergence cannot be claimed for any of the investigated reference space methods. The relations to the MFE methods are used to explain the loss of convergence.

Wheeler was partially supported by NSF grant DMS 0411413 and the DOE grant DE-FGO2-04ER25617. Yotov was supported in part by the DOE grant DE-FG02-04ER25618, the NSF grant DMS 0411694 and the J. Tinsley Oden Faculty Fellowship, The University of Texas at Austin.

I. Aavatsmark (✉) · G. T. Eigestad · R. A. Klausen
Centre for Integrated Petroleum Research,
University of Bergen, P.O. Box 7800, 5020 Bergen, Norway
e-mail: ivar.aavatsmark@cipr.uib.no

G. T. Eigestad
e-mail: geirte@mi.uib.no

R. A. Klausen
Centre of Mathematics for Applications, University of Oslo,
Mail: CMA, P.O. Box 1053 Blindern, 0316 Oslo, Norway
e-mail: runhildk@ifi.uio.no

M. F. Wheeler
Institute for Computational Engineering and Sciences
(ICES), Department of Aerospace Engineering &
Engineering Mechanics, and Department of Petroleum and
Geosystems Engineering, The University of Texas at Austin,
Austin, TX 78712, USA
e-mail: mfw@ices.utexas.edu

I. Yotov
Department of Mathematics, 301 Thackeray Hall,
University of Pittsburgh, Pittsburgh, PA 15260, USA
e-mail: yotov@math.pitt.edu

Keywords Mixed finite element method ·
Multipoint flux approximation ·
Control-volume method

1 Introduction

We consider a control-volume discretization of the model equation

$$-\operatorname{div}(\mathbf{K} \operatorname{grad} p) = g \text{ on } \Omega \quad (1)$$

on a 2D quadrilateral grid. The coefficient \mathbf{K} is a symmetric and positive definite tensor.

Our applications are flow in porous media, i.e., subsurface flow simulation. These equations contain an elliptic operator similar to the left-hand side of Eq. 1, and this motivates our study. The equations

have properties that constrain the choice of grid and discretization technique used for the elliptic operator. For multiphase flow, some variables (saturations) behave like solutions of hyperbolic equations, while one variable (the pressure) behaves like a solution of an elliptic equation. Phase transitions, which are strongly pressure-dependent, may occur.

Due to the hyperbolicity and the strongly nonlinear behavior of the saturations, the discretization scheme should be locally conservative. Also, because the phase transitions are pressure-dependent, the pressure should be evaluated at the same point as the saturations. This motivates the use of a control-volume scheme for Eq. 1, with evaluation of the dependent variable p at the centers of the cells.

Stability for the variables with hyperbolic behavior may be accomplished by upstream weighting of the phase flow. In a fully implicit scheme for the flow equations, a simple upstream weighting can be achieved if the method for the elliptic operator in Eq. 1 yields the flux at the edges as an explicit function of the potential p at some neighboring cell centers.

The absolute permeability may vary strongly in subsurface rocks. Because the potential node should be located at the cell centers, it is important that the discrete resistance between two nodes honors the strong heterogeneity.

The multipoint flux approximation (MPFA) method is a control-volume method that is designed to satisfy the properties described above. It can be applied to quadrilateral grids [1, 3, 5, 6, 17] and to unstructured grids [2, 4, 15, 30], see Aavatsmark [1] for a more complete bibliography. For quadrilateral grids, the method may be applied in the physical space or in a reference space. The physical-space approximations have good convergence properties [6], but are non-symmetric for quadrilaterals which are not parallelograms. In this paper, we consider the MPFA method for quadrilateral grids in a reference space [1, 5, 23, 24] and its relationship to the mixed finite element (MFE) method [12].

It is well known that the MFE methods are also locally mass conservative and compute fluxes on the edges. Two other closely related methods that handle rough grids and coefficients accurately are the control volume mixed finite element method [13] and the mimetic finite difference (MFD) method [21]. All three methods require the solution of a saddle point problem. A relationship between MFE methods and cell-centered finite difference (CCFD) methods via a quadrature rule was established in Russell and Wheeler [27] and explored in Weiser and Wheeler [31] to analyze convergence of pressure and velocity in CCFD methods on rectangular grids and diagonal tensor

coefficients. Another approach based on a relationship between MFE and a control volume method is discussed in Agouzal et al. [7]. An extension to full tensors and general grids was established through the expanded mixed finite element (EMFE) method [8, 9]. The EMFE method is superconvergent for smooth grids and coefficients but loses accuracy near discontinuities unless a hybrid formulation is employed or discontinuous elements are imposed. A discussion of the need for discontinuous elements for EMFE and a connection between these elements and MPFA is shown in Klausen and Russell [23]. The MPFA method combines the advantages of the previously mentioned methods—it is accurate for rough coefficients and grids and leads to a control-volume formulation with a cell-centered local pressure system.

In the MPFA method on quadrilateral grids in a reference space, the Jacobian matrix of the transformation is not constant. We discuss the different variants of the method that appear when the Jacobian matrix is evaluated at some naturally chosen points, namely, the midpoints and the corner points. On unstructured grids, these ideas have been suggested by Edwards [14, 16]. We also discuss the relationship between these MPFA variants and MFE methods using the Raviart–Thomas elements RT_0 [26] or the Brezzi–Douglas–Marini elements BDM_1 [11] with quadrature and how different choices of points in the quadrature rule give different versions of symmetric MPFA methods. Ideas using quadrature rules to establish a relationship between MFE methods and MPFA methods have been suggested by Edwards [15]. An advantage of the MFE formulations is that variational techniques can be employed to analyze the algebraic system and convergence properties of the MPFA method [22, 24, 32, 33].

The rest of the paper is organized as follows. In the next section, we present the reference-space MPFA method. The RT_0 and BDM_1 MFE formulations and their relationship to the MPFA method are discussed in Section 3. Numerical results for the convergence of the resulting MPFA versions are presented in Section 4. The paper ends with some conclusions in Section 5.

2 Multipoint flux approximation

The MPFA discretization approach is based on a control-volume formulation of the pressure Eq. 1, where more than two pressure values are used in the flux approximation for each edge of the control volume. The basic idea for the MPFA discretization is to divide each control-volume grid-cell into subcells and then assume linear variation of the pressure in each

subcell. All subcells with a common corner create a dual grid. The cells in the dual grid are denoted as interaction volumes, see Fig. 1. An interaction volume will hence contain four subedges when the mesh consists of quadrilaterals. Discrete fluxes are calculated for these edges. The flux across each subedge is determined from Darcy’s law on the linear pressure variation in each subcell. The discretization is accomplished by assuming continuous fluxes across each of the subedges and a weak continuity condition of the pressure across the same edges. From these assumptions, an explicit discrete flux can be found after eliminating the edge pressure for each subedge in an interaction volume.

Each subedge flux u_e can then be written explicitly as a weighted sum of the cell pressures of the interaction volume,

$$u_e = \sum_{i \in I} t_{e,i} p_i. \tag{2}$$

The coefficients $t_{e,i}$ are called the transmissibility coefficients associated with edge e , and I denotes the interaction volume. The transmissibilities are, in general, given by matrix expressions, but are easily found numerically.

In the following, we will deal with the MPFA O-method in a reference space [1]. The same continuity principles as in the physical space are then applied. However, the permeability is transformed into a tensor, which embodies the permeability and the geometry of the cell. The Jacobian matrix of this transformation is, in general, not constant, and this implies that the MPFA methods in the physical space and in the reference space are not identical.

The MPFA method in the physical space honors the exact geometry of the cell. This gives good convergence properties [6]. However, the matrix of coefficients of the resulting system of equations is nonsymmetric.

The MPFA method in the reference space is always symmetric. However, evaluation of the Jacobian matrix at discrete points implies that the geometry of the cell is only approximately honored, and, as will be seen, this yields less robust convergence properties on rough grids.

For parallelogram-shaped cells, the Jacobian matrix is constant and the two methods become identical. In

Fig. 1 Control volumes (solid) and interaction volumes (dashed)

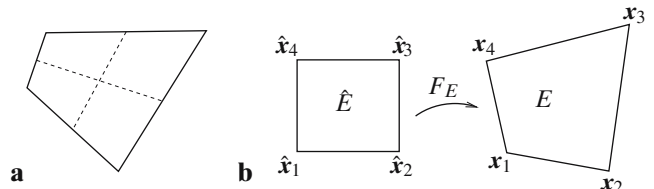
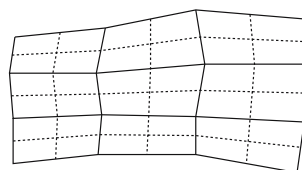


Fig. 2 **a** A control-volume grid cell and its subcells. **b** The bilinear mapping F_E from \hat{E} into E

this case, good convergence properties and symmetry are achieved.

2.1 Quadrilateral meshes

Let $\{\mathcal{T}_h\}$ denote a family of partitions of Ω into quadrilateral subdomains, or cells (control volumes), where h is the maximum element edge length. Assume that each interior corner of \mathcal{T}_h meets four cells. Further divide all the cells into four subcells by dividing each control-volume edge into two equal edges and using the intersection of the two straight dashed lines that connect opposite points in Fig. 2a. The control-volume edge partitions are denoted as half edges throughout this paper. Finally, denote the set of edges of \mathcal{T}_h by \mathcal{E}_h .

For any cell $E \in \mathcal{T}_h$, we will utilize a bilinear mapping $F = F_E : \hat{E} \rightarrow E$, which is smooth and invertible, see Fig. 2b. Here, the reference element $\hat{E} = (0, 1) \times (0, 1)$ is the unit square. Let $\mathbf{x}_i = (x_i, y_i)$, $i = 1, 2, 3, 4$, be the four corners of element E in counterclockwise direction as shown in Fig. 2b. If $\mathbf{x}_{ij} = (\mathbf{x}_i - \mathbf{x}_j)$, the transformation F takes the form

$$F(\hat{x}, \hat{y}) = \mathbf{x}_1 + \mathbf{x}_{21}\hat{x} + \mathbf{x}_{41}\hat{y} + (\mathbf{x}_{32} - \mathbf{x}_{41})\hat{x}\hat{y}, \tag{3}$$

for $(\hat{x}, \hat{y}) \in \hat{E}$. The Jacobian matrix of F is denoted $\mathbf{D} = \mathbf{D}_E$, and $J = J_E$ is the Jacobian of the mapping.

A quadrilateral $E \in \{\mathcal{T}_h\}$ is said to be a h^2 -parallelogram if there exists a constant C independent of h such that

$$|F_{\hat{x}\hat{y}}| = |\mathbf{x}_{32} - \mathbf{x}_{41}| \leq Ch^2. \tag{4}$$

Given a general quadrilateral grid, this is a consequence of uniform refinement. This condition is necessary to achieve superconvergence for the MFE method, cf. Ewing et al. [20]. The MFE method is locally conservative and symmetric and can hence serve as a reference for expected behavior for locally conservative methods. We will see numerically that, on h^2 parallelograms, the symmetric reference-space MPFA method gives the same order of convergence as the MFE method with the lowest-order Raviart–Thomas elements, $O(h^2)$, for both pressure and flux.

Define the analogous permeability in the reference space

$$\hat{\mathbf{K}} = \mathbf{J}\mathbf{D}^{-1}\mathbf{K}\mathbf{D}^{-\mathbf{T}}. \tag{5}$$

Note that $\hat{\mathbf{K}}$ is symmetric and positive definite for each \mathbf{x} . If $\hat{\mathbf{K}}$ is diagonal for all $E \in \mathcal{T}_h$, the grid is denoted a \mathbf{K} -orthogonal grid.

The analogous permeability embodies both the permeability and the shape of the cells. The discrete pressure and flux values from the reference space remain unchanged compared to the discrete values in the physical space; $\hat{p} = p \circ F_E(\hat{\mathbf{x}})$. If \mathbf{n}_e denotes the edge unit normal, we have

$$u_e = - \int_e \mathbf{K} \text{grad } p \cdot \mathbf{n}_e \, ds = - \int_{\hat{e}} \hat{\mathbf{K}} \text{grad } \hat{p} \cdot \hat{\mathbf{n}}_e \, d\hat{s} = \hat{u}_e \tag{6}$$

with $\hat{\mathbf{K}}$ defined by Eq. 5. For quadrilateral grids, the analogous permeability $\hat{\mathbf{K}}$ in the reference space will not be cell-wise constant even if the physical permeability is constant.

2.2 The MPFA method

Here, we derive the MPFA method in a formulation that will match the MFE method. In this form, the explicit MPFA flux is found after inverting a local 4×4 matrix. Note that $\hat{\mathbf{K}}$ is independent of any translation of the reference mapping F_E , see Eq. 3. The reference mapping can therefore be adjusted for four cells with one common corner, so that we have a reference interaction volume, \hat{I} . This adjustment does not affect any of the transformed quantities.

The MPFA method can be derived locally on each interaction volume. We consider one interaction volume, where the cell and half edges are numbered from 1 to 4, see Fig. 3.

For each subcell E_i , we evaluate the tensor $\hat{\mathbf{K}}$ at a point, to get a constant tensor on each subcell. The constant subcell approximation of $\hat{\mathbf{K}}|_{E_i}$ is denoted by \mathcal{K}_{E_i} , and the components of \mathcal{K}_E^{-1} are denoted κ_{ij}^E , $i, j = 1, 2$. Define the pressure space $P(\hat{I})$ on the interaction

volume \hat{I} to be linear on each subcell \hat{E}_i and to be continuous on the boundary of \hat{I} . For each $\hat{p} \in P(\hat{I})$, let $\{p_k\}_{k=1,2,3,4}$ be the values of \hat{p} at the corners of \hat{I} and let $\{\lambda_k\}_{k=1,2,3,4}$ be the values of \hat{p} at the midpoints of the boundary edges of \hat{I} , see Fig. 3. The local pressure \hat{p} is then uniquely defined by the eight degrees of freedom $\{p_k, \lambda_k\}$. Let

$$u_e|_{E_i} = -\mathcal{K}_{E_i} \text{grad } \hat{p}|_{E_i} \cdot \hat{\mathbf{n}}_e / 2 \tag{7}$$

for the four inner subcell edges. The MPFA pressure space P_{MPFA} on \hat{I} is further restricted to

$$P_{\text{MPFA}}(\hat{I}) = \{\hat{p} \in P(\hat{I}) : [u_e]_e = 0, \forall e \in \mathcal{E}^{1/2}(\hat{I})\}, \tag{8}$$

where $\mathcal{E}^{1/2}(\hat{I})$ means the four inner edges of \hat{I} , $[\cdot]_e$ is the jump across edge e , and u_e is defined by Eq. 7. The pressure $\hat{p} \in P_{\text{MPFA}}(\hat{I})$ is then uniquely determined by the cell pressures $\{p_k\}_{k=1,2,3,4}$, cf. Klausen and Winther [24].

To illustrate the mixed form of the discrete equations, we follow a procedure from Aavatsmark et al. [5], Edwards [15], and Klausen and Winther [24]. Consider the two subcells 1 and 2 with node pressures p_1 and p_2 and their common upper half edge e_1 , see Fig. 3. Subcell 1 then connects the half edges e_1 and e_4 . Calculating the flux for half edge e_1 and e_4 with Darcy’s law on subcell 1, gives

$$u_{e_1} = -\frac{1}{2}\mathcal{K}_1 \text{grad}(\hat{p}) \cdot \begin{bmatrix} 1 \\ 0 \end{bmatrix}, \quad u_{e_4} = -\frac{1}{2}\mathcal{K}_1 \text{grad}(\hat{p}) \cdot \begin{bmatrix} 0 \\ 1 \end{bmatrix}, \tag{9}$$

or,

$$(\mathcal{K}_1)^{-1} \begin{bmatrix} u_{e_1} \\ u_{e_4} \end{bmatrix} = -\frac{1}{2} \text{grad}(\hat{p}). \tag{10}$$

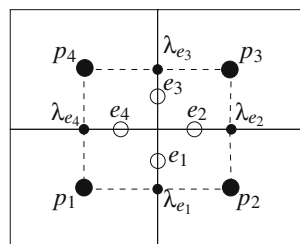
Next, $\text{grad}(\hat{p})$ is determined from the assumption of linear pressure variation in each subcell. In the reference space, the constant gradient is determined in each subcell between the node pressure and one point on each half edge. Let p_1 be the node pressure of cell 1 and let the pressure at the midpoint of the actual edge be λ_{e_1} , see Fig. 3. This gives

$$\begin{aligned} -\frac{1}{2} \text{grad}(\hat{p})|_{\hat{E}_1} &= \begin{bmatrix} p_1 - \lambda_{e_1} \\ p_1 - \lambda_{e_4} \end{bmatrix}, \\ -\frac{1}{2} \text{grad}(\hat{p})|_{\hat{E}_2} &= \begin{bmatrix} \lambda_{e_1} - p_2 \\ p_2 - \lambda_{e_2} \end{bmatrix}. \end{aligned} \tag{11}$$

Eliminating λ_{e_1} from Eq. 11 and the constant gradient values by Eq. 10 gives

$$(\kappa_{11}^1 + \kappa_{11}^2)u_{e_1} + \kappa_{12}^1 u_{e_4} + \kappa_{12}^2 u_{e_2} = -(p_2 - p_1). \tag{12}$$

Fig. 3 Four cells, numbered 1 to 4, and their common interaction volume in the reference space, where large dots denote the cell pressures $\{p_i\}$ and the small dots the edge pressure $\{\lambda_{e_i}\}$



On each interaction volume, the left-hand side of Eq. 12 can be written as the first row in

$$A[u_{e_1}, u_{e_2}, u_{e_3}, u_{e_4}]^T, \tag{13}$$

where

$$A = \begin{bmatrix} (\kappa_{11}^1 + \kappa_{11}^2) & \kappa_{12}^2 & 0 & \kappa_{12}^1 \\ \kappa_{12}^2 & (\kappa_{22}^2 + \kappa_{22}^3) & \kappa_{12}^3 & 0 \\ 0 & \kappa_{12}^3 & (\kappa_{11}^3 + \kappa_{11}^4) & \kappa_{12}^4 \\ \kappa_{12}^1 & 0 & \kappa_{12}^4 & (\kappa_{22}^1 + \kappa_{22}^4) \end{bmatrix}. \tag{14}$$

Similar equations for the other subedges yields the other rows of the expression Eq. 13. By inspection, this is a symmetric positive definite matrix if and only if $(\kappa_E^i)^{-1}$, $i = 1, 2, 3, 4$, is symmetric positive definite. Inverting this matrix on each interaction volume gives the explicit flux and transmissibility coefficients traditionally found for MPFA in the literature. Symmetry and positive definiteness of the final matrix of coefficients were first shown by Aavatsmark et al. [5] for the midpoint evaluation case. The symmetry of the final matrix of coefficients follows from the symmetry of the local 4×4 matrix associated with each interaction volume. Because \hat{K} is symmetric and positive definite for all \hat{x} , approximation by any point values on each subcell maintains this symmetry. In the numerical section, we show different behavior for MPFA for the different approximation points.

2.3 Midpoint and corner-point Jacobian evaluations

For general quadrilaterals, the Jacobian matrix and its determinant are not constant. They are evaluated at a point to retain the property that the transformed permeability tensor is constant on each subcell. Depending on the point at which the matrix is evaluated, methods with different properties appear. Relations to quadrature rules in MFE formulations will be discussed in Section 3.3. Below, we discuss how the treatment in the reference space approximates the treatment in

the physical space for two different evaluations. The chosen evaluation points of the Jacobian matrix are the cell center and the cell corners. More precisely, the Jacobian matrix for each subcell is evaluated at either the center or the corner in the interaction volume.

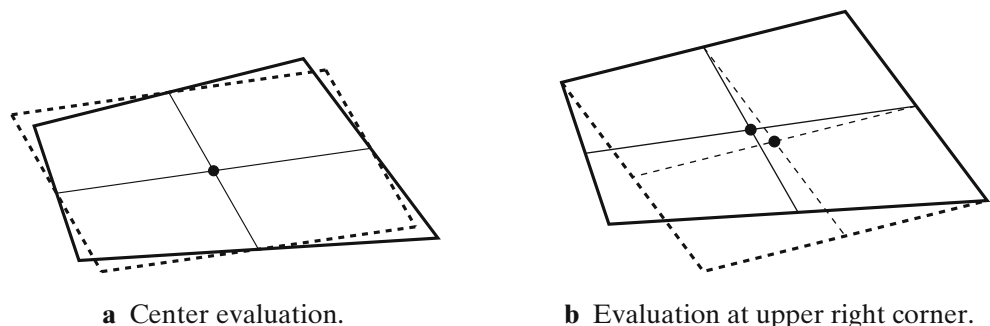
Consider the quadrilateral (solid lines) of Fig. 4. The lines connecting the midpoints of opposite edges are drawn. Their intersection defines the center of the cell. Evaluating the Jacobian matrix at the cell center corresponds to replacing the quadrilateral with the dashed parallelogram shown in Fig. 4a. Thus, a center evaluation of the Jacobian matrix corresponds to the case in which the distances from the cell center to the edge midpoints are correct but where the edges of the corresponding parallelogram have wrong orientation and length.

To get a correct orientation of the edges, one may instead evaluate the Jacobian matrix at the corner in the interaction volume that is treated [14, 16]. This guarantees that the edges used for the flux calculation in this interaction volume have correct orientation and length. The parallelogram corresponding to this evaluation of the Jacobian matrix is shown with dashed lines in Fig. 4b. Obviously, the cell center of the parallelogram has now moved away from the cell center of the original quadrilateral. However, the choice of a cell-center point is not crucial for the behavior of the method [6]. The difficulty here is therefore that the parallelograms of the different corners have different cell centers. This implies that the resistance through a cell may be either too large or too small. In Section 4 the center-evaluation and the corner-evaluation methods are compared with the method in the physical space.

3 The MFE method

In this section, we discuss MPFA written as a MFE method with a numerical quadrature rule. From this point of view, different natural choices of the point evaluation for \hat{K} follow from the quadrature rule.

Fig. 4 Replacing a quadrilateral (solid) by its associated parallelogram (dashed)



The unknown fluid velocity \mathbf{u} is now introduced in the system of equations, which leads to the classical mixed formulation of Eq. 1,

$$\mathbf{u} = -\mathbf{K} \operatorname{grad} p, \quad \operatorname{div} \mathbf{u} = g. \tag{15}$$

Assuming a boundary condition $p = 0$ on $\partial\Omega$, a weak formulation of the system Eq. 15 can be formulated as the problem of finding $(\mathbf{u}, p) \in H(\operatorname{div}) \times \mathcal{L}_2$ such that

$$\begin{aligned} (\mathbf{K}^{-1}\mathbf{u}, \mathbf{v}) - (p, \operatorname{div} \mathbf{v}) &= 0 && \text{for all } \mathbf{v} \in H(\operatorname{div}), \\ (\operatorname{div} \mathbf{u}, q) &= (g, q) && \text{for all } q \in \mathcal{L}_2, \end{aligned} \tag{16}$$

where

$$H(\operatorname{div}) = \{\mathbf{v} \in (\mathcal{L}_2)^2 : \operatorname{div} \mathbf{v} \in \mathcal{L}_2\}$$

and g is assumed to be a \mathcal{L}_2 function.

The MFE method is a discrete version of this system: find $(\mathbf{u}_h, p_h) \in \mathbf{V}_h \times Q_h \subset H(\operatorname{div}) \times \mathcal{L}_2$ such that

$$\begin{aligned} (\mathbf{K}^{-1}\mathbf{u}_h, \mathbf{v}) - (p_h, \operatorname{div} \mathbf{v}) &= 0 && \text{for all } \mathbf{v} \in \mathbf{V}_h, \\ (\operatorname{div} \mathbf{u}_h, q) &= (g, q) && \text{for all } q \in Q_h, \end{aligned} \tag{17}$$

where the finite element spaces \mathbf{V}_h and Q_h can be one of two sets of elements introduced in the next subsections.

3.1 Broken Raviart–Thomas elements

These elements are introduced and analyzed in Klausen and Russell [23] and Klausen and Winther [24], and the connection between the MFE method with these elements and the MPFA method is shown there. The basic ideas for the connection and analysis were presented in Klausen [22].

Let a, b, c , and d be piecewise constant functions on $(0, 1)$, with a discontinuity at $1/2$. On the reference square \hat{E} , the velocity functions $\hat{\mathcal{R}}\mathcal{T}_0^{1/2}$ are defined as the eight-dimensional space given by

$$\hat{\mathcal{R}}\mathcal{T}_0^{1/2} := \begin{bmatrix} a(\hat{y}) + b(\hat{y})\hat{x} \\ c(\hat{x}) + d(\hat{x})\hat{y} \end{bmatrix}.$$

For comparison, the classical Raviart–Thomas functions $\hat{\mathcal{R}}\mathcal{T}_0$, cf. [12], are given when a, b, c , and d are constants on the entire cell \hat{E} , so $\hat{\mathcal{R}}\mathcal{T}_0 \subset \hat{\mathcal{R}}\mathcal{T}_0^{1/2}$. It is straightforward to check that, if $\hat{\mathbf{v}} \in \hat{\mathcal{R}}\mathcal{T}_0^{1/2}$ and $\hat{\mathbf{n}}$ is a normal vector to an edge of \hat{E} , then $\hat{\mathbf{v}} \cdot \hat{\mathbf{n}}$ is a constant along each half edge. Furthermore, this property is preserved by the Piola transformation for each cell. If

$\hat{\mathbf{v}}$ is a vector field in $H(\operatorname{div}, \hat{E})$, define a vector field \mathbf{v} on E by the Piola transformation $\mathcal{P} = \mathcal{P}_E$ [29], i.e.,

$$\mathbf{v}(\mathbf{x}) = \mathcal{P}\hat{\mathbf{v}}(\mathbf{x}) = \frac{1}{J} \mathbf{D}\hat{\mathbf{v}} \circ F^{-1}(\mathbf{x}).$$

The velocity space, $\mathcal{RT}_0^{1/2} \subset H(\operatorname{div})$, is now defined by

$$\mathcal{RT}_0^{1/2} := \{\mathbf{v} \in H(\operatorname{div}) : \mathbf{v}|_E \in \mathcal{P}_E(\hat{\mathcal{R}}\mathcal{T}_0^{1/2}), \quad \forall E \in \mathcal{T}_h\}.$$

The pressure is approximated by piecewise constants on \mathcal{T}_h , i.e., we let

$$Q_h := \{q \in \mathcal{L}_2 : q|_E \in P_0(E), \quad \forall E \in \mathcal{T}_h\}, \tag{18}$$

where P_k denotes the space of polynomials of degree $\leq k$.

3.2 Brezzi–Douglas–Marini elements

In Wheeler and Yotov [32, 33], a multipoint flux MFE method that reduces to CCFDs on simplicial and curvilinear quadrilateral grids via quadrature rule was introduced and analyzed. There it was shown that this method, based on the lowest-order Brezzi–Douglas–Marini BDM_1 MFE spaces, is closely related to the MPFA method.

On the reference unit square, the BDM_1 spaces are defined as [11, 12]

$$\begin{aligned} \mathcal{BD}\hat{\mathcal{M}}_1 &:= P_1(\hat{E})^2 + r \operatorname{curl}(\hat{x}\hat{y}) + s \operatorname{curl}(\hat{x}\hat{y}^2) \\ &= \begin{bmatrix} \alpha_1\hat{x} + \beta_1\hat{y} + \gamma_1 + r\hat{x}^2 + 2s\hat{x}\hat{y} \\ \alpha_2\hat{x} + \beta_2\hat{y} + \gamma_2 - 2r\hat{x}\hat{y} - s\hat{y}^2 \end{bmatrix}, \quad \hat{Q} := P_0(\hat{E}), \end{aligned} \tag{19}$$

where $\alpha_1, \alpha_2, \beta_1, \beta_2, \gamma_1, \gamma_2, r, s$ are constants. Note that $\operatorname{div} \mathcal{BD}\hat{\mathcal{M}}_1 = \hat{Q}$ and that for all $\hat{\mathbf{v}} \in \mathcal{BD}\hat{\mathcal{M}}_1$ and for any edge \hat{e} of \hat{E}

$$\hat{\mathbf{v}} \cdot \hat{\mathbf{n}}_{\hat{e}} \in P_1(\hat{e}).$$

The degrees of freedom for $\mathcal{BD}\hat{\mathcal{M}}_1$ can be chosen to be the values of $\hat{\mathbf{v}} \cdot \hat{\mathbf{n}}_{\hat{e}}$ at any two points on each edge \hat{e} . We choose these points to be the vertices of \hat{e} . This choice is motivated by the requirement of accuracy and certain orthogonalities for the quadrature rule discussed below.

The velocity BDM_1 space on \mathcal{T}_h is defined via the Piola transformation:

$$\mathcal{BDM}_1 = \{\mathbf{v} \in H(\operatorname{div}) : \mathbf{v}|_E \in \mathcal{P}_E(\mathcal{BD}\hat{\mathcal{M}}_1), \quad \forall E \in \mathcal{T}_h\}. \tag{20}$$

The pressure BDM₁ space consists of piecewise constants, i.e., it coincides with the RT₀ pressure space Q_h defined in Eq. 18.

3.3 The quadrature rule

To obtain the MPFA method as a MFE method, we need to replace the term $(\mathbf{K}^{-1}\mathbf{u}_h, \mathbf{v})_E$ in Eq. 17 by a quadrature formula. We define this numerical quadrature formula on the reference element \hat{E} and denote it $\hat{a}_{\hat{E}}(\cdot, \cdot)$.

We note that if $\hat{\mathbf{K}}|_{\hat{E}} = \mathbf{J}\mathbf{D}^{-1}\mathbf{K}\mathbf{D}^{-T}$, then $\hat{\mathbf{K}}^{-1}|_{\hat{E}} = \mathbf{J}^{-1}\mathbf{D}^T\mathbf{K}^{-1}\mathbf{D}$ and

$$(\mathbf{K}^{-1}\mathbf{u}, \mathbf{v})_E = \left(\mathbf{J}\mathbf{K}^{-1} \frac{1}{J}\mathbf{D}\hat{\mathbf{u}}, \frac{1}{J}\mathbf{D}\hat{\mathbf{v}} \right)_{\hat{E}} = \left(\hat{\mathbf{K}}^{-1}\hat{\mathbf{u}}, \hat{\mathbf{v}} \right)_{\hat{E}} \tag{21}$$

for all $\mathbf{u}, \mathbf{v} \in \mathbf{V}_h$.

The first part of the quadrature rule is the approximation of $\hat{\mathbf{K}}$ by a constant tensor \mathcal{K}_{E_i} on each subcell E_i . To get the MPFA method as defined in, for instance, Aavatsmark [1], we evaluate $\hat{\mathbf{K}}(\hat{\mathbf{x}})$ at the midpoint of each reference element. Another, and equally natural, approximation is to evaluate $\hat{\mathbf{K}}$ at the corners of the cell. This corresponds to evaluating the normal components of $\hat{\mathbf{K}}$ at the edges, which is where we actually calculate the fluxes. As we will see in the numerical section, the edge evaluation is better than the midpoint evaluation. Other evaluation points for $\hat{\mathbf{K}}$ have also been tested, like, for instance, the Gaussian points [10], but they have not performed as well as the corner evaluation.

Let $\hat{E}_i, i = 1, 2, 3, 4$, denote the four subcells of \hat{E} , and let e_{ij} denote the outer half edge of subcell \hat{E}_i with the j th unit vector as a normal, cf. Fig. 5. In the quadrature rule, we will use \mathcal{K}_{E_i} to approximate $\hat{\mathbf{K}}$. The second part of the quadrature formula is derived from the trapezoidal rule, cf. Klausen and Winther [24] or Wheeler and Yotov [33].

Application of the trapezoidal quadrature rule in both directions requires the evaluation of the vectors at the corners. We note that a vector at a corner is

uniquely determined by the values of its normal components to the edges intersecting at this corner. For any $\hat{\mathbf{v}} = (\hat{v}_1, \hat{v}_2) \in \hat{\mathbf{V}}$, the vector at a corner $\hat{\mathbf{x}}_i$ is

$$\hat{\mathbf{v}}(\hat{\mathbf{x}}_i) = \begin{bmatrix} \hat{v}_{i1} \\ \hat{v}_{i2} \end{bmatrix},$$

where $\hat{v}_{ik} = \hat{v}_k(\hat{\mathbf{x}}_i), k = 1, 2$. For $\hat{\mathbf{v}} \in \hat{\mathcal{R}}\mathcal{T}^{1/2}$, the components \hat{v}_{ik} are not merely the corner values $\hat{v}_k(\hat{\mathbf{x}}_i)$ but also $\hat{v}_{ik} = \hat{v}_k|_{e_{ik}}, k = 1, 2$. Note that we have thus associated with each corner $\hat{\mathbf{x}}_i$, two basis functions of $\hat{\mathbf{V}}$, namely $\hat{\mathbf{v}}_{ik}$ corresponding to the degrees of freedom $\hat{v}_{ik}, k = 1, 2$.

Following the discussion above, we now define for $\hat{\mathbf{u}}, \hat{\mathbf{v}} \in \hat{\mathbf{V}}$,

$$\hat{a}_{\hat{E}}(\hat{\mathbf{u}}, \hat{\mathbf{v}}) = \frac{1}{4} \sum_{i=1}^4 \mathcal{K}_{E_i}^{-1} \hat{\mathbf{u}}(\hat{\mathbf{x}}_i) \cdot \hat{\mathbf{v}}(\hat{\mathbf{x}}_i) = \frac{1}{4} \sum_{i=1}^4 \sum_{j,k=1}^2 \kappa_{jk}^{E_i} \hat{u}_{ij} \hat{v}_{ik}, \tag{22}$$

where $\kappa_{jk}^{E_i}$ are the components of $\mathcal{K}_{E_i}^{-1}$. Clearly, the quadrature rule Eq. 22 only couples the two basis functions $\hat{\mathbf{v}}_{ik}, k = 1, 2$, associated with a corner $\hat{\mathbf{x}}_i$ of \hat{E} . For example, for a corner $\hat{\mathbf{x}}_i$,

$$\begin{aligned} \hat{a}_{\hat{E}}(\hat{\mathbf{v}}_{i1}, \hat{\mathbf{v}}_{ik}) &= \frac{1}{4} \kappa_{1k}^{E_i}, \quad k = 1, 2, \quad \text{and} \\ \hat{a}_{\hat{E}}(\hat{\mathbf{v}}_{i1}, \hat{\mathbf{v}}_{jk}) &= 0, \quad j \neq i, k = 1, 2. \end{aligned} \tag{23}$$

For a discussion of the quality of this numerical integration used with midpoint evaluation of $\hat{\mathbf{K}}$ in the case of $\mathbf{V}_h = \mathcal{RT}_0^{1/2}$, see Klausen and Winther [24]. For a discussion of the approximation qualities of the corner based evaluation in the case of $\mathbf{V}_h = \mathcal{BDM}_1$, see Wheeler and Yotov [32, 33].

Finally, define the perturbed bilinear form

$$a_h(\mathbf{u}, \mathbf{v}) = \sum_{\mathcal{T}_h} \hat{a}_{\hat{E}}(\hat{\mathbf{u}}, \hat{\mathbf{v}}) \tag{24}$$

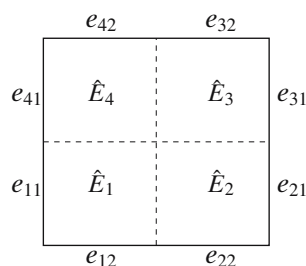
for all $\mathbf{u}, \mathbf{v} \in \mathbf{V}_h$.

Remark 3.1 The quadrature rule Eq. 22 is closely related to an inner product used in the MFD methods [21], where the integration is performed in the physical space. We note that it is simpler to evaluate the quadrature rule on the reference element \hat{E} .

3.4 The MPFA method from the MFE method

The last step of rewriting the MPFA method as a perturbed MFE method is to apply the quadrature rule on Eq. 17. With the quadrature rules Eq. 24 used to

Fig. 5 One cell, with four subcells \hat{E}_i , and the half cell edges e_{ij}



perturb Eq. 17, we have defined the finite element method: find $(\mathbf{u}_h, p_h) \in \mathbf{V}_h \times Q_h$ such that

$$\begin{aligned} a_h(\mathbf{u}_h, \mathbf{v}) - (p_h, \operatorname{div} \mathbf{v}) &= 0 \quad \text{for all } \mathbf{v} \in \mathbf{V}_h, \\ (\operatorname{div} \mathbf{u}_h, q) &= (g, q) \quad \text{for all } q \in Q_h. \end{aligned} \tag{25}$$

It is shown in Klausen and Winther [24] and Wheeler and Yotov [33] for $\mathbf{V}_h = \mathcal{RT}_0^{1/2}$ and $\mathbf{V}_h = \mathcal{BDM}_1$, respectively, that the method Eq. 25 has a unique solution.

Proposition 3.1 For either $\mathbf{V}_h = \mathcal{RT}_0^{1/2}$ or $\mathbf{V}_h = \mathcal{BDM}_1$, method Eq. 25 is equivalent to the MPFA method presented in Section 2.2.

Proof First note that there is a one-to-one correspondence between the degrees of freedom of $\mathbf{V}_h \times Q_h$ and the unknowns in the MPFA method. Recall that only the two basis functions associated with a corner of \hat{E} are coupled by the quadrature rule Eq. 22, see Eq. 23. Therefore, for any interior vertex of T_h , taking $\mathbf{v} = \mathbf{v}_1, \mathbf{v}_2, \mathbf{v}_3, \mathbf{v}_4$, the four associated basis functions in Eq. 25, leads to a 4×4 local system for the four unknown velocities u_1, u_2, u_3, u_4 . A simple calculation shows that, in the reference space, this system is identical to the MPFA system Eqs. 12–14. \square

The following properties of the local and global systems follow easily from the variational formulation Eq. 25.

Proposition 3.2 The local 4×4 velocity linear systems and the resulting global cell-centered pressure system are symmetric and positive definite.

Proof Denoting by $\{\mathbf{v}_i\}$ and $\{q_j\}$ the bases of \mathbf{V}_h and Q_h , respectively, the algebraic system that arises from Eq. 25 is

$$\begin{pmatrix} \mathbf{A} & \mathbf{B}^T \\ \mathbf{B} & \mathbf{O} \end{pmatrix} \begin{pmatrix} \mathbf{u} \\ \mathbf{p} \end{pmatrix} = \begin{pmatrix} \mathbf{0} \\ \mathbf{g} \end{pmatrix}, \tag{26}$$

where $A_{ij} = a_h(\mathbf{v}_i, \mathbf{v}_j)$ and $B_{ij} = -(q_j, \operatorname{div} \mathbf{v}_i)$. The matrix \mathbf{A} is block-diagonal with 4×4 diagonal blocks. The symmetry of \mathbf{A} is obvious. It is easy to check that because \mathbf{K} is symmetric and positive definite, $a_h(\cdot, \cdot)$ is a norm in \mathbf{V}_h , and therefore, each diagonal block of \mathbf{A} is symmetric and positive definite. The elimination of \mathbf{u} in Eq. 26 leads to the system $\mathbf{B}\mathbf{A}^{-1}\mathbf{B}^T \mathbf{p} = -\mathbf{g}$. We have that $\mathbf{B}^T \mathbf{p} = \mathbf{0}$ implies $\mathbf{p} = \mathbf{0}$. This can be shown by using the inf-sup condition

$$\forall q \in Q_h, \quad \sup_{\mathbf{0} \neq \mathbf{v} \in \mathbf{BDM}_1} \frac{(q, \operatorname{div} \mathbf{v})}{\|\mathbf{v}\|_{\operatorname{div}}} \geq \beta \|q\|.$$

Therefore, $\mathbf{B}\mathbf{A}^{-1}\mathbf{B}^T$ is symmetric and positive definite. \square

Remark 3.2 Note that only homogeneous pressure boundary conditions have been treated in this section. In general, for the different formulations, the naturally derived boundary conditions will not necessarily be equal.

4 Numerical experiments

In this section, we test \mathcal{L}_2 convergence properties of the MPFA O-method which, is based on a mapping onto a reference space. By Proposition 3.1, this method yields the same discrete solution as the two methods derived in Section 3. The results are compared to the physical-space discretization. The benefit of using a reference

Fig. 6 Random orthogonal grid (a) and the uniformly refined grid (b)

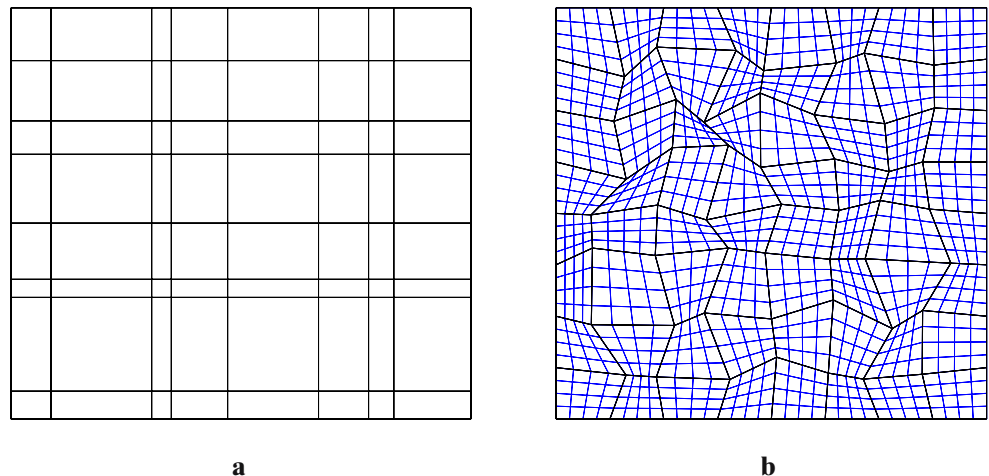
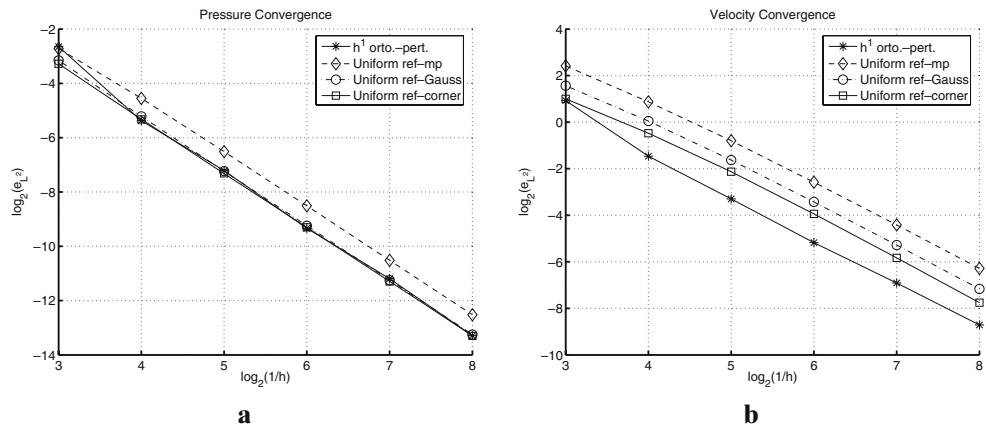


Fig. 7 Convergence behavior for MPFA on the grids shown in Fig. 6. For the uniform refined grid, the reference space is used with midpoint, Gaussian point, and corner-point evaluation of the permeability. **a** Pressures. **b** Normal velocities



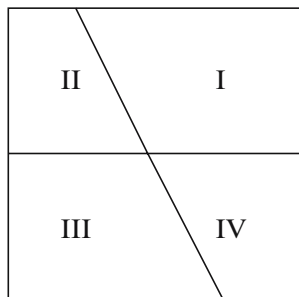
space is a symmetric mass matrix. It will be shown when this gives the same order of convergence as the discretization in the physical space and when more care has to be taken when choosing which MPFA version to use.

Significant numerical testing has been done for the MPFA O-method in the physical space in Aavatsmark et al. [6], Eigestad et al. [18], and Eigestad and Klausen [19]. Test examples therein cover both smooth and nonsmooth grids and cases with discontinuous permeability. Examples in 2D are provided in Eigestad et al. [18] and Eigestad and Klausen [19], whereas both 2D and 3D results are given in Aavatsmark et al. [6]. The convergence rates are estimated from numerical experiments. We make use of the interpolated Hilbert space H^ξ where ξ is a positive real number, see Chapter 8 in Strang and Fix [28]. If the potential is in $H^{1+\alpha}$, $\alpha > 0$, the obtained \mathcal{L}_2 convergence order on rough grids in the physical space is $\min\{2, 2\alpha\}$ for the potential and $\min\{1, \alpha\}$ for the normal velocities. For smooth grids, the convergence order for the normal velocities increases to $\min\{2, \alpha\}$.

4.1 Homogeneous medium; smooth solutions

We first discuss the convergence behavior for a smooth reference solution on a homogeneous medium. The first test case has a permeability tensor with eigenvalues 10

Fig. 8 Case with four subdomains



and 1, where the eigenvectors are rotated 30° counter-clockwise. This gives

$$K = \begin{bmatrix} 7.7500 & 3.8971 \\ 3.8971 & 3.2500 \end{bmatrix}.$$

Equation 1 is solved on the domain $(0, 1) \times (0, 1)$ with Dirichlet boundary conditions. The boundary conditions and the source term in Eq. 1 are chosen to correspond to the solution

$$p(x, y) = \cos(2\pi x) \cos(2\pi y). \tag{27}$$

Our first grid is an orthogonal grid that is constructed from a uniform distribution of orthogonal grid cells, where all corners with the same i and j indices are perturbed randomly by a factor in $[-0.35h, 0.35h]$ in x and y directions, respectively, see Fig. 6a. On orthogonal grids, the Jacobian matrix is constant, and hence, all considered MPFA methods are identical. They give second-order convergence for both pressure and velocity on these grids.

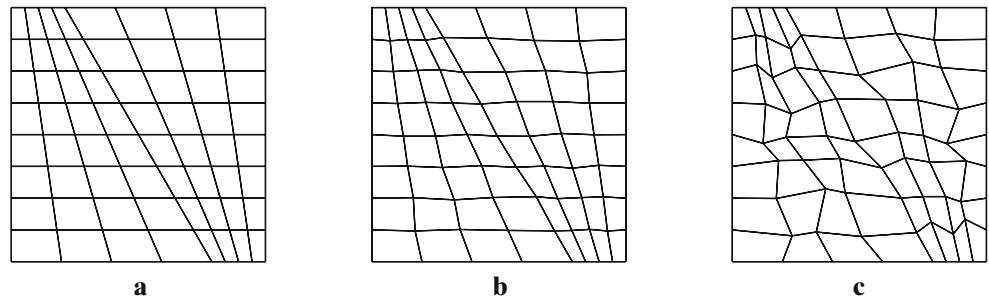
The next grid is a uniform refinement of a rough initial grid, see Fig. 6b. On this grid, the evaluation of \hat{K} is taken in the midpoint of the cell, in the Gaussian points, and in the corner of the grid cells, respectively. All examples give second-order convergence for both pressure and normal velocity, and the results are shown in Fig. 7. The smallest error is obtained for the corner-point evaluation of the permeability.

We next test the solution

$$p(x, y) = \cos(\pi x) \cosh(\pi y) \tag{28}$$

for the physical-space discretization and for the reference-space discretization with midpoint evaluation and corner-point evaluation of \hat{K} on a sequence of skew grids. The permeability is $K = I$, and suitable Dirichlet boundary conditions are applied on the boundary of the domain $(0, 1) \times (0, 1)$. The chosen

Fig. 9 Grids used for simulations. **a** Smooth grid. **b** Random h^2 perturbation of the smooth grid. **c** Random h^1 perturbation of the smooth grid



grids have to account for an inner grid line rotated 120° from the horizontal line, see Fig. 8.

The unperturbed grid is depicted in Fig. 9a. Perturbations of the grid cells by h^ν will be used in the numerical tests. This means that each corner (x_i, y_i) of the grid is transformed to

$$\tilde{x}_i = x_i + R_{x,i}h^\nu, \quad \tilde{y}_i = y_i + R_{y,i}h^\nu,$$

where $R_{x,i}, R_{y,i}$ are random numbers between -0.5 and 0.5 . These perturbations are performed at each refinement level, and the grids are denoted h^ν -perturbed grids. In the tests, both h^2 and h^1 perturbations are used in the refinements of the grids, see Fig. 9.

The pressure convergence rate for all the discretizations is $O(h^2)$ for h^2 -perturbed grids, see Fig. 10a. For h^1 perturbation of the grids, the pressure still converges with rate $O(h^2)$ for the physical-space discretization, whereas the convergence diminishes or vanishes for the reference-space discretizations. In the last refinement level, the errors are only reduced by $O(h^{0.5})$ for the corner-point evaluation. The same behavior is seen for the midpoint evaluation. This agrees with the results reported by Mishev [25]. It is hence not possible to conclude that the pressure converges asymptotically for rough grids.

The normal-velocity behavior is illustrated in Fig. 10b. For uniform refinement of the grids, the convergence for all MPFA versions is second order.

Furthermore, the rates of convergence are close to second order for h^2 perturbations for the discretization in the physical space. There is an apparent difference between the discretizations for h^2 perturbations of the grid. As seen from Fig. 10b, one order is lost for the normal velocities for the discretization in the reference space when the reference permeability is evaluated in the midpoint. When the reference permeabilities are evaluated at the corners of the subcells of the interaction volumes, close to $O(h^2)$ convergence is regained, which shows the improvements this method has over the conventional midpoint evaluation.

The difference in convergence behavior becomes critical for h^1 perturbed grids. In the physical space, the convergence rate of the normal velocities is decreased to h^1 . Both the midpoint evaluation and the corner-point evaluation of the reference permeability yield no convergence of the normal velocities. It should be noted that the errors are smaller for the corner-point evaluation than for the midpoint evaluation.

4.2 Discontinuous coefficients

When subdomains with different permeabilities meet, nonsmooth solutions may be constructed. In Fig. 8, we may take the medium to consist of either four subdomains, where opposite pairs have the same permeability, or two subdomains with the same permeability.

Fig. 10 Convergence behavior of Eq. 28 for discretizations in the physical space and in the reference space with midpoint and corner-point evaluation. The grids are shown in Fig. 9. **a** Pressures. **b** Normal velocities

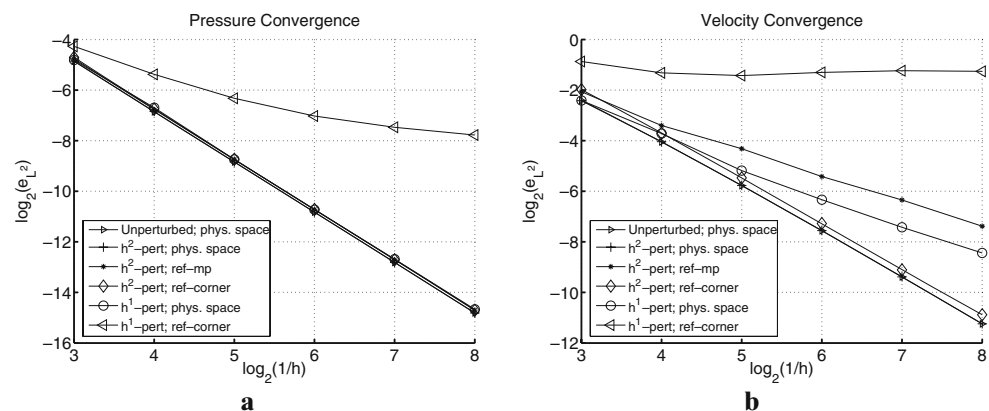
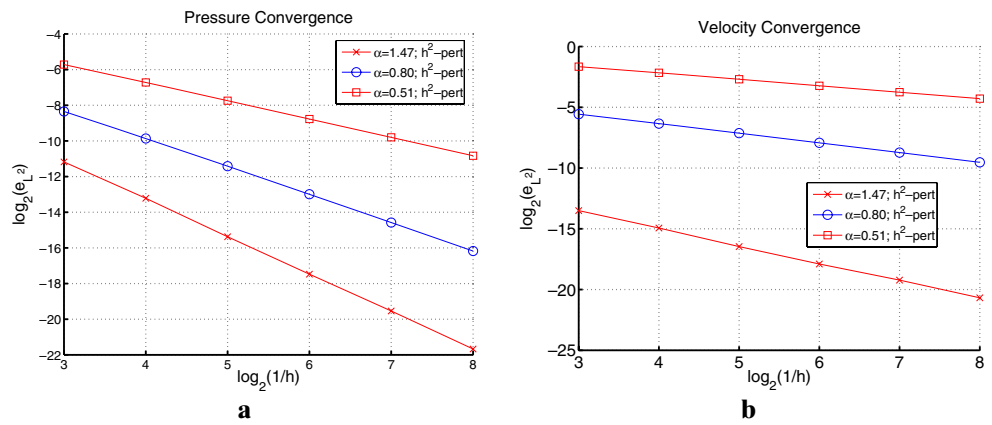


Fig. 11 Convergence behavior for h^2 perturbations in the physical space for solutions with reduced regularity. *Left:* pressures. *Right:* normal velocities



The physical-space-based MPFA method for such cases is broadly discussed in Eigestad and Klausen [19] and Aavatsmark et al. [6]. Solutions in the space $H^{1+\alpha}$ are tested, where α takes the values 1.47, 0.80, and 0.51, respectively. These pressure solutions are given by Aavatsmark et al. [6]

$$p(r, \theta) = r^\alpha (a_i \cos(\alpha\theta) + b_i \sin(\alpha\theta)),$$

where a change to polar coordinates is introduced. The discretization methods are tested for convergence for different perturbations of the grid in Fig. 9. The case where $\alpha = 1.47$ arises for the permeability contrast $k_{\Omega_1}/k_{\Omega_2} = 10^{-3}$, where the domain Ω_1 is the domain I in Fig. 8, and Ω_2 comprises the rest of the domain, see Fig. 8. The other two examples use four subdomains where diagonally opposite subdomains have the same permeability.

The results for the discretization in the physical space for h^2 perturbations are depicted in Fig. 11 and may be compared to the results in Fig. 12 where the same examples are investigated for the discretization in the reference space for both the midpoint evaluation and the corner-point evaluation of the reference permeability. The pressure convergence rate is

$O(h^{\min\{2, 2\alpha\}})$ for all discretizations when the grids are h^2 -perturbed. As seen from the two plots, the convergence rate for the normal velocities for the case $\alpha = 1.47$ is $O(h^\alpha)$ in the physical space, whereas it is only $O(h^1)$ for the midpoint evaluation in the reference space. The corner-point evaluation of the reference permeability regains $O(h^\alpha)$ convergence for the normal velocity. For the two cases where $\alpha < 1$, both the physical-space discretization and the reference-space discretizations are $O(h^\alpha)$ convergent for the normal velocities.

When h^1 perturbations are introduced, much the same conclusions as for the homogeneous case hold for the discontinuous case. The three different cases of varying α s are depicted in Fig. 13 for the three different discretization alternatives. The pressures for the discretizations in the reference space seem to converge in the earliest refinement steps and then gradually decrease, similar to the behavior for the smooth solution. The pressure is $O(h^{\min\{2, 2\alpha\}})$ -convergent for the physical-space discretization.

As seen from the plots for the normal velocities, the convergence rate in the physical space for the normal velocities is $O(h^{\min\{1, \alpha\}})$, whereas the discretizations in

Fig. 12 Convergence behavior for h^2 perturbations of the grid for solutions with reduced regularity. Discretizations in the reference space with midpoint and corner-point evaluation. *Left:* pressures. *Right:* normal velocities

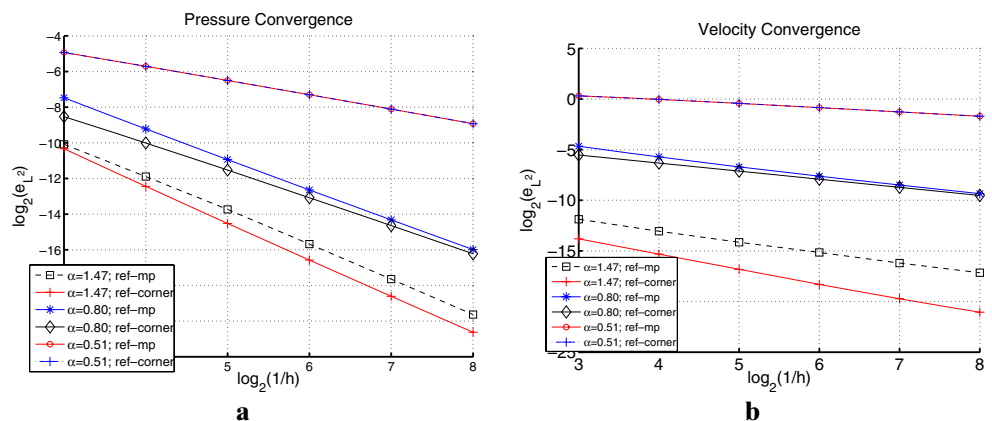
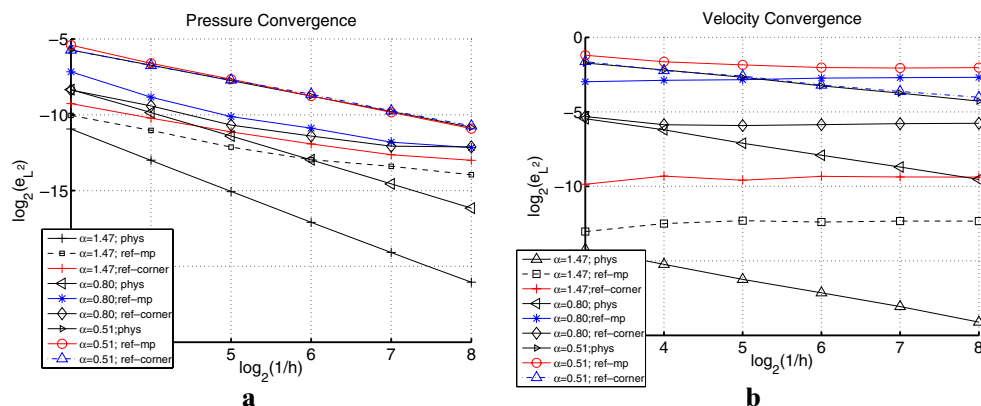


Fig. 13 Convergence behavior for h^1 perturbations of the grid for solutions with reduced regularity. Discretizations in the physical space and in the reference space with midpoint and corner-point evaluation. *Left:* pressures. *Right:* normal velocities



the reference space are not convergent. Note, however, that the case $\alpha = 0.51$ seems to yield a small order of convergence for the velocities when the corner-point evaluation of the reference permeability is employed. Our explanation for this is the fact that leading errors occur near the discontinuity lines and the corner points on this line are unperturbed to account for the physical edges. The corner-point evaluation then seems to perform better because the h^1 perturbations are not felt locally. This is merely an artifact of the special geometry of the example.

Summing up, the new corner-point evaluation of the permeability performs just as well as the physical-space discretization on uniform refined grids or when only h^2 perturbations exist in the grid. This is in contrast to the midpoint evaluation, where, for solutions in $H^{1+\alpha}$, $\alpha > 1$, the convergence order of the normal velocities is reduced by $\min\{1, \alpha - 1\}$. When the grids have h perturbations at all refinement levels, convergence is, in general, lost for the discretizations in the reference space.

5 Conclusions

We presented two MFE formulations, broken RT_0 and BDM_1 , of the reference-space MPFA method on quadrilateral grids. A trapezoidal-type quadrature rule reduces the velocity mass matrix to a block-diagonal form and leads to a symmetric positive definite cell-centered pressure system. Two types of transformed permeability evaluations, midpoint and corner-point, lead to two MPFA method variants. The numerical experiments indicate that the corner-point evaluation is generally more accurate than the midpoint evaluation. For h^2 -perturbed meshes, the corner-point gives $O(h^2)$ convergence for the velocity, while the midpoint gives only $O(h)$ convergence. This is related to the fact that the former approach results in applying the trapezoidal quadrature rule for integrating $\hat{\mathbf{K}}\hat{\mathbf{u}} \cdot \hat{\mathbf{v}}$. On h^1 -perturbed

meshes, however, both reference-space methods suffer reduction or loss of convergence, which is not the case for the physical-space MPFA method. The reason for the reduced convergence on rough grids is that the approximation properties of the MFE spaces and the accuracy of the quadrature rule on quadrilateral grids depend on the smoothness of the Piola mapping. These results are consistent with the theoretical results obtained in Klausen [22], Klausen and Winther [24], and Wheeler and Yotov [32, 33].

References

- Aavatsmark, I.: An introduction to multipoint flux approximations for quadrilateral grids. *Comput. Geosci.* **6**, 404–432 (2002)
- Aavatsmark, I., Barkve, T., Bøe, Ø., Mannseth, T.: A class of discretization methods for structured and unstructured grids in anisotropic, inhomogeneous media. In: Heinemann, Z., Kriebner, M. (eds.) *Proceedings of the 5th European Conference on the Mathematics of Oil Recovery*, pp. 157–166. Leoben, Austria (1996)
- Aavatsmark, I., Barkve, T., Bøe, Ø., Mannseth, T.: Discretization on non-orthogonal, quadrilateral grids for inhomogeneous, anisotropic media. *J. Comput. Phys.* **127**, 2–14 (1996)
- Aavatsmark, I., Barkve, T., Bøe, Ø., Mannseth, T.: Discretization on unstructured grids for inhomogeneous, anisotropic media. Part I: derivation of the methods. Part II: discussion and numerical results. *SIAM J. Sci. Comput.* **19**, 1700–1736 (1998)
- Aavatsmark, I., Barkve, T., Mannseth, T.: Control-volume discretization methods for 3D quadrilateral grids in inhomogeneous, anisotropic reservoirs. *SPE J.* **3**, 146–154 (1998)
- Aavatsmark, I., Eigestad, G.T., Klausen, R.A.: Numerical convergence of the MPFA O-method for general quadrilateral grids in two and three dimensions. In: Arnold, D.N., Bochev, P.B., Lehoucq, R.B., Nicolaides, R.A., Shashkov, M. (eds.) *Compatible Spatial Discretizations*, vol. 142 of IMA Vol. Ser., pp. 1–21. Springer, New York (2006)
- Agouzal, A., Baranger, J., Maitre, J.-F., Oudin, F.: Connection between finite volume and mixed finite element methods for a diffusion problem with nonconstant coefficients.

- Application to a convection diffusion problem. *East-West J. Numer. Math.* **3**, 237–254 (1995)
8. Arbogast, T., Dawson, C.N., Keenan, P.T., Wheeler, M.F., Yotov, I.: Enhanced cell-centered finite differences for elliptic equations on general geometry. *SIAM J. Sci. Comput.* **19**, 404–425 (1998)
 9. Arbogast, T., Wheeler, M.F., Yotov, I.: Mixed finite elements for elliptic problems with tensor coefficients as cell-centered finite differences. *SIAM J. Numer. Anal.* **34**, 828–852 (1997)
 10. Björk, Å., Dahlquist, G.: *Numerical Methods*. Prentice-Hall, Englewood Cliffs (1974)
 11. Brezzi, F., Douglas, J. Jr., Marini, L.D.: Two families of mixed elements for second order elliptic problems. *Numer. Math.* **88**, 217–235 (1985)
 12. Brezzi, F., Fortin, M.: *Mixed and Hybrid Finite Element Methods*. Springer, New York (1991)
 13. Cai, Z., Jones, J.E., McCormick, S.F., Russell, T.F.: Control-volume mixed finite element methods. *Comput. Geosci.* **1**, 289–315 (1997)
 14. Edwards, M.G.: Symmetric positive definite general tensor discretization operators on unstructured and flow based grids. In: *Proceedings of the 8th European Conference on the Mathematics of Oil Recovery*, Freiberg, Germany, E04 (2002)
 15. Edwards, M.G.: Unstructured, control-volume distributed, full-tensor finite-volume schemes with flow based grids. *Comput. Geosci.* **6**, 433–452 (2002)
 16. Edwards, M.G.: Control-volume distributed sub-cell flux schemes for unstructured and flow based grids. In: *Proceedings of SPE Reservoir Simulation Symposium*, Houston, TX, SPE 79710 (2003)
 17. Edwards, M.G., Rogers, C.F.: Finite volume discretization with imposed flux continuity for the general tensor pressure equation. *Comput. Geosci.* **2**, 259–290 (1998)
 18. Eigestad, G.T., Aadland, T., Aavatsmark, I., Klausen, R.A., Nordbotten J.M.: Recent advances for MPFA methods. In: *Proceedings of the 9th European Conference on the Mathematics of Oil Recovery*, Cannes, France, B002 (2004)
 19. Eigestad, G.T., Klausen, R.A.: On the convergence of the multi-point flux approximation O-method; numerical experiments for discontinuous permeability. *Numer. Methods Partial Differ. Equ.* **21**, 1079–1098 (2005)
 20. Ewing, R.E., Liu, M.L., Wang, J.: Superconvergence of mixed finite element approximations over quadrilaterals. *SIAM J. Numer. Anal.* **36**, 772–787 (1999)
 21. Hyman, J.M., Shashkov, M., Steinberg, S.: The numerical solution of diffusion problems in strongly heterogeneous non-isotropic materials. *J. Comput. Phys.* **132**, 130–148 (1997)
 22. Klausen, R.A.: On locally conservative numerical methods for elliptic problems; application to reservoir simulation. Dissertation, No 297, University of Oslo (2003)
 23. Klausen, R.A., Russell, T.F.: Relationships among some locally conservative discretization methods which handle discontinuous coefficients. *Comput. Geosci.* **8**, 341–377 (2004)
 24. Klausen, R.A., Winther, R.: Convergence of multipoint flux approximations on quadrilateral grids. *Numer. Methods Partial Differ. Equ.* **22**, 1438–1454 (2006)
 25. Mishev, I.D.: Nonconforming finite volume methods. *Comput. Geosci.* **6**, 253–268 (2002)
 26. Raviart, P.-A., Thomas, J.-M.: A mixed finite element method for 2nd order elliptic problems. In: *Mathematical Aspects of the Finite Element Method*, Lecture Notes in Mathematics, vol. 606, pp. 292–315. Springer, New York (1977)
 27. Russell, T.F., Wheeler, M.F.: Finite element and finite difference methods for continuous flows in porous media. In: Ewing, R.E. (ed.) *The Mathematics of Reservoir Simulation*, *Frontiers in Applied Mathematics*, vol. 1, pp. 35–106. SIAM, Philadelphia (1983)
 28. Strang, W.G., Fix, G.J.: *An Analysis of the Finite Element Method*. Prentice-Hall, Englewood Cliffs (1973)
 29. Thomas, J.-M.: *Sur l'analyse numérique des méthodes d'éléments finis hybrides et mixtes*, thèse de doctorat d'état, Université Pierre et Marie Curie, Paris VI (1977)
 30. Verma, S., Aziz, K.: Two- and three-dimensional flexible grids for reservoir simulation. In: Heinemann, Z., Kriebner, M. (eds.) *Proceedings of the 5th European Conference on the Mathematics of Oil Recovery*, pp. 143–156. Leoben, Austria (1996)
 31. Weiser, A., Wheeler, M.F.: On convergence of block-centered finite-differences for elliptic problems. *SIAM J. Numer. Anal.* **25**, 351–375 (1988)
 32. Wheeler, M.F., Yotov, I.: A cell-centered finite difference method on quadrilaterals. In: Arnold, D.N., Bochev, P.B., Lehoucq, R.B., Nicolaides, R.A., Shashkov, M. (eds.) *Compatible Spatial Discretizations*, IMA Vol. Ser., vol. 142, pp. 189–207. Springer, New York (2006)
 33. Wheeler, M.F., Yotov, I.: A multipoint flux mixed finite element method. *SIAM J. Numer. Anal.* **44**, 2082–2106 (2006)